Control methodology and implementation of a Z-source inverter for a stand-alone photovoltaic-diesel generator-energy storage system microgrid

Ahmed Belila, El-Madjid Berkouk, Mohamed Benbouzid, Yassine Amirat, Bekheira Tabbache, Abdeslam Mamoune

Control Methodology and Implementation of a Z-Source Inverter for a Stand-Alone Photovoltaic-Diesel Generator-Energy Storage System Microgrid

Ahmed Belila[a,c], El-Madjid Berkouk[b], Mohamed Benbouzid[c,d], Yassine Amirat[e], Bekheira Tabbache[a], Abdeslam Mamoune[c]

[a] *Ecole Militaire Polytechnique, UER ELT, 16111 Algiers, Algeria.*
[b] *Ecole Nationale Polytechnique, LCP-lab, 16000 Algiers, Algeria.*
[c] *University of Brest, UMR CNRS 6027 IRDL, 29238 Brest, France*
[d] *Shanghai Maritime University, 201306 Shanghai, China.*
[e] *ISEN Yncrea Ouest Brest, UMR CNRS 6027 IRDL, 29200 Brest, France.*

Abstract

This paper deals with the control and implementation of a bidirectional Z-source inverter for a photovoltaic -diesel generator-energy storage hybrid system. The proposed control strategy is based on the voltage regulation across one of the Z-network capacitor (V_{cz}), through a buck-boost converter of the storage system side. In some critical situations, where the load power is important, the V_{cz} voltage regulation is no longer able to ensure the duration of the necessary state shoot-through for the maximum power point tracking achievement. In this context, the diesel generator can therefore be solicited to ensure the shoot-through duration and achieve maximum power point tracking so that it can be used more advantageously without any harmful effects on the Z-source inverter operation. The effectiveness of the proposed control strategy is evaluated and validated by extensive simulations and experiments.

Keywords: Microgrid, hybrid system, Z-source inverter, photovoltaic generator, diesel generator, energy storage system, maximum power point tracking (MPPT).

*Corresponding author
*mohamed.benbouzid@univ-brest.fr

List of Symbols

PVG-DG	PV Generator-Diesel Generator
ESS	Energy Storage System
RMS	Root Mean Square
PLL	Phase-Locked Loop
PCC	Point of Common Coupling
AVR	Automatic Voltage Regulation
ZSI	Z-source inverter
PI	Proportional Integral
MPPT	Maximum Power Point Tracking
T_v	Valve actuator time-constant
T_d	Diesel engine time-constant
T_0	Shoot-through time interval
I	Switching cycle time
B	Boost factor
G	voltage gain of the ZSI
D	Shoot-through duty ratio
PWM	Pulse Width Modulation
D_0	Maximum value of D
S-T	Shoot-through
M	modulation index
MBC	Maximum Boost Control

VOC Voltage Oriented Control

V_i DC-link voltage

1. Introduction

Hybrid systems photovoltaic-diesel generator-energy storage system (PV-DG-ESS), are one of the most promising microgrids for the electrical energy production due to their low environmental impact and high availability of solar irradiation in most geographical locations[1, 2]. Conventional parallel configuration of PVG-DG-ESS power systems uses typically a two-stage power conversion topology (Fig.1). The first stage provides the DC/DC power conversion from the PVG to a DC-link energy buffer (such as a capacitor), and the second stage provides the DC/AC power conversion from the energy buffer to the AC bus[3]. For better performance, the DG is connected to the AC bus in a parallel configuration [4, 5].

The hight dependence of the energy generated by the PVG to the environmental operating conditions, such as the solar irradiance level and the panel temperature, requires to use a DC/DC converter controlled by an MPPT technique to extract the maximum available energy [6]. On the other hand and in order to ensure the same voltage amplitude at the AC bus with DG output voltages, an Energy Storage System (ESS) is generally used to regulate the DC bus voltage through a buck-boost converter [7] (Fig.1). This DC bus voltage must be regulated at a high voltage level -according to the adopted switching strategy- in order to ensure a value of 220 volts RMS on the AC bus.

The issue of the DC bus voltage step-up can be solved using single-stage converter, such as the Z-source inverter (ZSI), instead of a two-stage converter one [8]. The ZSI has been widely introduced in the literatture as a competitive alternative to existing inverter topologies for various applications. Some works have proposed new control methods, analysis, and structures with improved features of the ZSI [9, 10, 11, 12]. In other paper works, this type of converter has gained tremendous interest in photovoltaic conversion systems to acheive

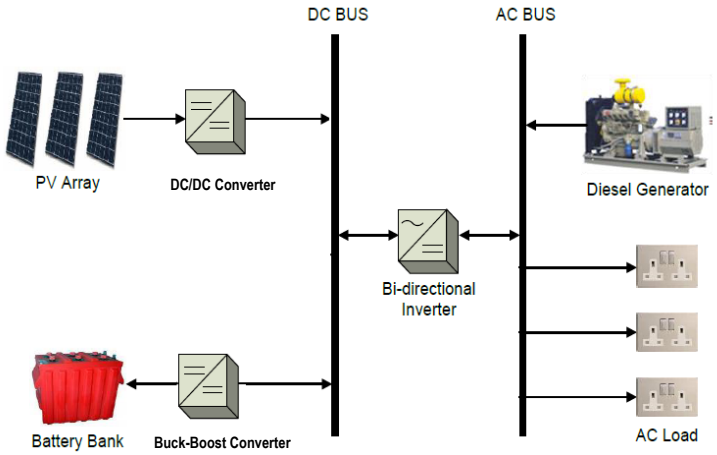

Figure 1: Traditional PVG-DG-ESS system.

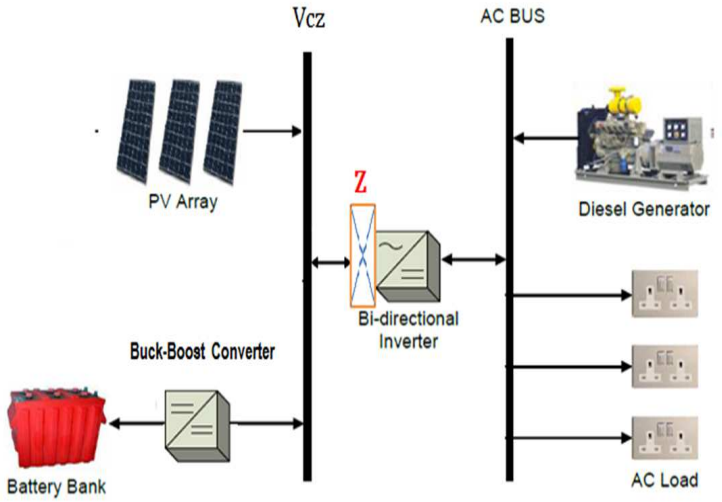

Figure 2: PVG-DG-ESS system with a Z-source inverter.

the MPPT without the use of a DC/DC converter [2, 13, 14, 15]. As well as for electric vehicles aplications where it has been considered as a suitable solution to drive the traction motor and control the input power by one more control freedom: shoot-through state [16, 17, 18, 19].

For an autonomous hybrid PVG-DG-ESS power system, the output voltages of the ZSI must be regulated during a variation in the load power demand to ensure the voltage synchronization between the ZSI and the DG in the AC bus. This is reflected on the reference voltages amplitude variation and consequently on the modulation index M. By introducing the shoot-through mode, the ZSI can boost its input DC voltage, and subsequently its output AC voltages[20, 21], so as to optimize the system size and cost[22, 23]. This additional control degree of freedom offered by the shoot-through state is used to achieve the MPPT tracking and boost the input DC voltage. Indeed to keep constant the ZSI output voltage on AC bus (V_{AC}), amounts to:

- Either, adjusts the modulation index M.
- Either adjusts the voltage across the Z-source capacitor (V_{cz}).

Since any MPPT command in a PV system using ZSI is based on the use of the shoot-through state, the second adjustment remains the most common approach to track (${V_{PVG}}^*$) at the maximum power point (MPP). The Z-source capacitor voltage V_{cz} must be accordingly, increased/decreased according to the load requirement. In some critical situations when a peak load occurs, the decrease of the voltage V_{cz} results in a decrease of the ZSI output voltages.

The ZSI capacitor voltage (V_{cz}) regulation is one of the indirect control methods to control the DC-link voltage (V_i). This control method is simple and easy to implement with only one sensor. In some critical situations, when a peak load occurs or for fast changing input voltages, the peak DC-link voltage becomes uncontrollable while regulating the shoot-through duty cycle (D_0), this affects the output AC voltages [24].

To adress this issue, this paper proposes a new control strategy for an autonomous hybrid PVG-DG-ESS power system integrating a ZSI, where the DG can ensure shoot-through duration to achieve high performances of the ZSI in critical situations, so that it is utilized more advantageously without any harmful effects on the output AC voltages.

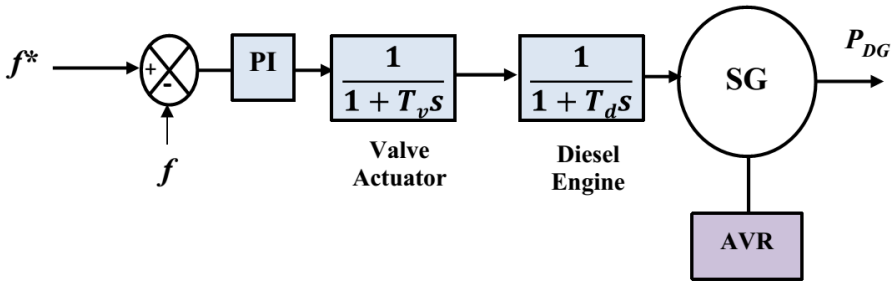

Figure 3: Block diagram of a diesel generator

This paper is organized as follows: Section 2 presents the system structure and modeling. Section 3 describes the proposed control strategy. Section 4 illustrates the effectiveness of the proposed technique with simulation results and Section 5 illustrates experimental results.

2. System Structure and Modeling

Figure 2 shows the structure of the parallel PVG-DG-ESS hybrid system using a ZSI, which boosts the source voltage by introducing the shoot-through state to achieve MPPT tracking. As this paper focuses on the control scheme of the ZSI and the DG, PVG and ESS sources modeling and sizing are beyond the scope of this paper. Their details can be found in [3, 4, 5, 7].

2.1. DG Model

The DG model, illustrated by Fig.3, is widely used and well-describes the dynamic behavior of small DG sets [25]. The valve actuator and the diesel engine are represented by first-order lags, with time-constants T_v and T_d, respectively. The speed governor is used to control the speed of the diesel engine and correspondingly the output frequency. The nominal output voltage is maintained by the automatic voltage regulation (AVR) [4, 25].

2.2. ZSI Modeling

The ZSI employs an impedance network consisting in two pairs of inductors and capacitors connected in an X shape, therefore achieving two functions

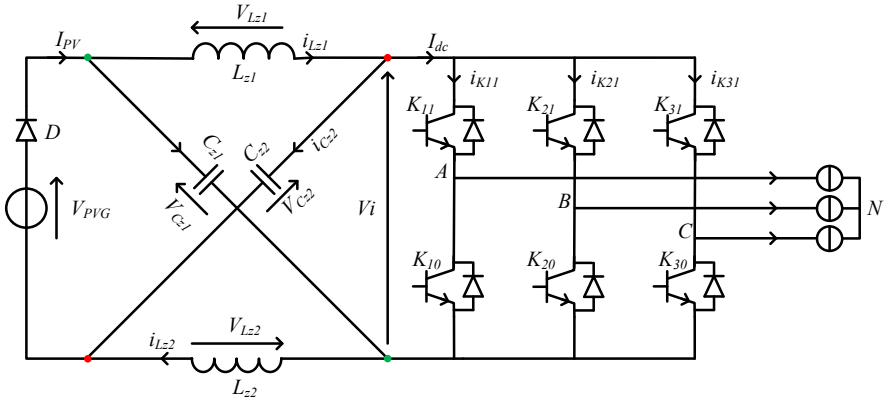

Figure 4: ZSI topology.

using the same converter circuit. The first one is similar to that of a boost converter, while the second one is identical to that of a conventional two-level inverter [26, 27]. The impedance network represents both an energy source and a filter for the converter where the inductance limits current ripples during the shoot-through state, while the capacitor is intended to absorb these ripples and maintains a constant voltage. For the ZSI analysis easiness, the AC side is considered to be equivalent to a current source (Fig.4). The impedance network offers the possibility of simultaneously closing the two switches of the same cell, which enables the ZSI boosting the output voltage [15]. Figure.5 illustrates the ZSI impedance network equivalent circuits during shoot-through and the active states.

The shoot-through time interval (T_0) over a switching cycle (T), determines the boost factor (B) and the voltage gain (G) of the ZSI, which can be expressed as follows[28]:

$$G = \frac{\hat{V}_{ac}}{V_{dc}/2} = BM = \frac{M}{1-2D} \tag{1}$$

Where $\hat{V}_{ac}$ is the peak value of the AC output voltage, V_{dc} is the input DC voltage, M is the modulation index and D is the shoot-through duty ratio ($D = T_0/T$). With a symmetric Z-source network ($L = L_1 = L_2$ and $C = C_1 =$

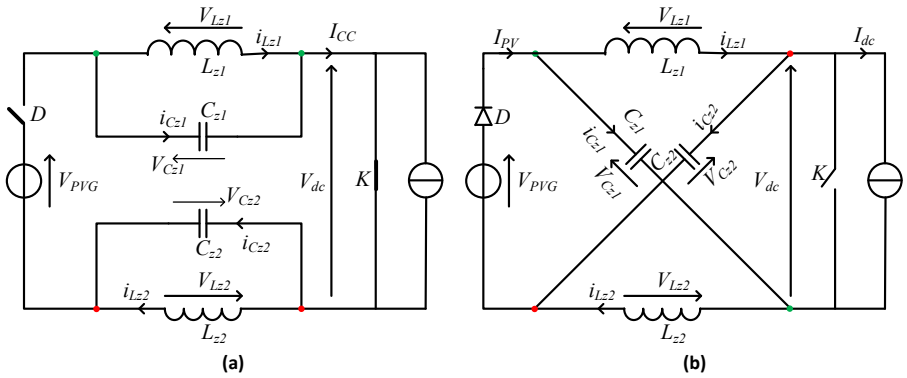

Figure 5: ZSI equivalent circuit. (a) Shoot-through states; (b) Active states.

C_2), the voltage across the Z-source capacitor can be expressed as follows[29]:

$$V_{cz} = \frac{(T - T_0)}{(T - 2T_0)} V_{PVG} \tag{2}$$

The peak value of the AC output voltage ($\hat{V_{AC}}$), can be controlled by varying M :

$$\hat{V_{ac}} = M \frac{V_{dc}}{2} \tag{3}$$

Assuming that F_{ij} represents the connection functions for each switch (K_{ij}):

$$\begin{cases} F_{ij} = 1 \rightarrow if : K_{i1} = 1 \\ F_{ij} = 0 \rightarrow if : K_{i1} = 0 \end{cases} \tag{4}$$

Thus, the output voltages of ZSI can be expressed in the following matrix form:

$$\begin{bmatrix} V_{an} \\ V_{bn} \\ V_{cn} \end{bmatrix} = \frac{1}{3} V_{dc} \begin{bmatrix} 2 & -1 & -1 \\ -1 & 2 & -1 \\ -1 & -1 & 2 \end{bmatrix} \cdot \begin{bmatrix} F_{11} \\ F_{21} \\ F_{31} \end{bmatrix} \tag{5}$$

3. Control scheme design

In the literature, several control methods have been proposed for ZSI PWM-based control [28, 30, 31]. To achieve maximum voltage boost, the maximum

boost control (MBC) method is adopted in this work, since it converts all traditional zero states to shoot-through, while maintaining unchanged the six active states (Fig.6). From Fig.6(a), the maximum value of the average shoot-through duty ratio D_0 can be expressed as follows:

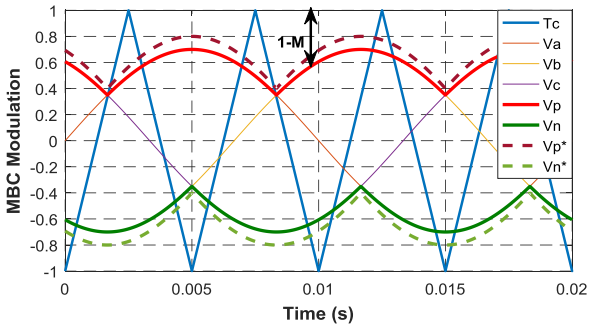

(a)

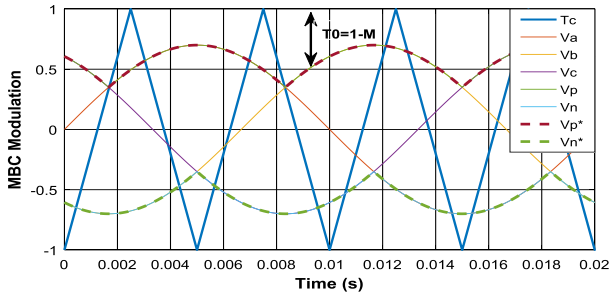

(b)

Figure 6: MBC control strategy: a) MBC in normal operation mode, b) MBC in critical operation mode.

$$D_0 = \int_{\pi/6}^{\pi/2} \frac{(2 - M\sin\theta - M\sin(\theta - 2\pi/3)}{2} d\theta = \frac{2\pi - 3\sqrt{3}M}{2\pi} \tag{6}$$

Therefore the boost factor (B) and the voltage gain (G) of the ZSI can be

expressed respectively as follows:

$$B = \frac{\pi}{3\sqrt{3}M - \pi} \tag{7}$$

$$G = \frac{\pi M}{3\sqrt{3}M - \pi} \tag{8}$$

The relationship between M and D_0 shows that when a peak load occurs, the modulation index M exceeds its maximum value, required to keep the additional control degree of freedom offered by the shoot-through states and consequently, the system can end up in a critical mode as shown by Fig.6(b).

To extract maximum power from the PVG, the Z-source capacitor voltage need to be boosted to the PVG voltage at the maximum power point MPP (${V_{pv}}^*$). Traditionally, the output of the MPPT controller is the reference signal for generating a shoot-through time interval (${T_0}^*$) to track the PVG voltage at the MPP. Equation 2 can now be rewritten as follows:

$${V_{cz}}^* = \frac{1 - D_0}{1 - 2D_0} {V_{PVG}}^* \tag{9}$$

Equation 9 clearly shows that MPPT tracking can be achieved by a judicious control of the (V_{cz}). Figure 7 shows the Perturb & Observ (P&O) algorithm based MPPT, which has two control loops: the outer loop tracks the MPP voltage (${V_{PVG}}^*$) and the the inner loop controls the courent i_{Lz}.

Since the voltage and the output current of the PVG vary according to the temperature and irradiation profile, the voltage of the Z-source capacitor (V_{cz}) is imposed through D, so that it can follow the variations of ${V_{PVG}}^*$. In normal operation mode when: $0 \leq D \leq D_0$, a shoot-through time interval (${T_0}^*$) is sufficient to acheive the MPPT. The V_{cz} voltage is therefore regulated at a reference voltage ${V_{cz}}^*$ to ensure a constant voltage in the AC bus.

When the T_0 period is not sufficient to achieve the MPPT, the ${V_{cz}}^*$ voltage need to be relatively smaller than V_{cz} ($D > D_0$) and the output voltage V_{ac} will be consequently impacted by this variation. This justifies that achieving

MPPT, using a ZSI converter, is subjected on an adequate system sizing that must be done beforehand[28].

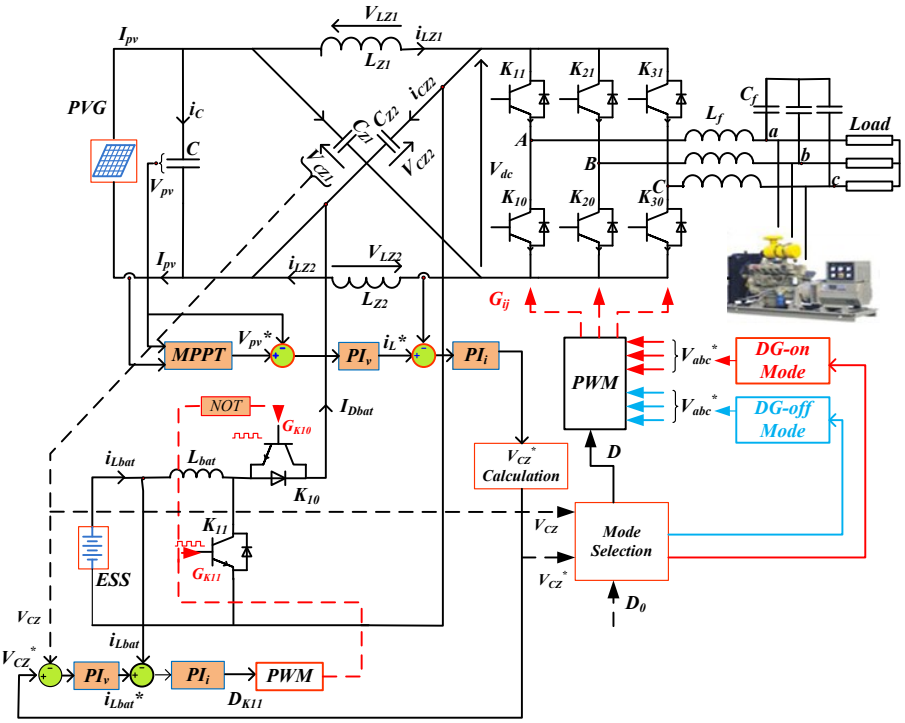

Figure 7: Proposed control scheme.

3.1. Z-Capacitor voltage regulation

The buck-boost converter that links the ESS to the ZSI capacitor provides an adjustable voltage at V_{cz} to ensure the MPPT tracking. Given its current reversibility, it ensures energy transfer to or from the battery to allows the ESS charging/discharging operation. As shown in Fig.8, the reversible buck-boost converter consists in two switches forming a switching cell. According to the energy flow, two possible configurations are distinguished, ESS charging and discharging. The average model of this converter in both configurations is as follows:

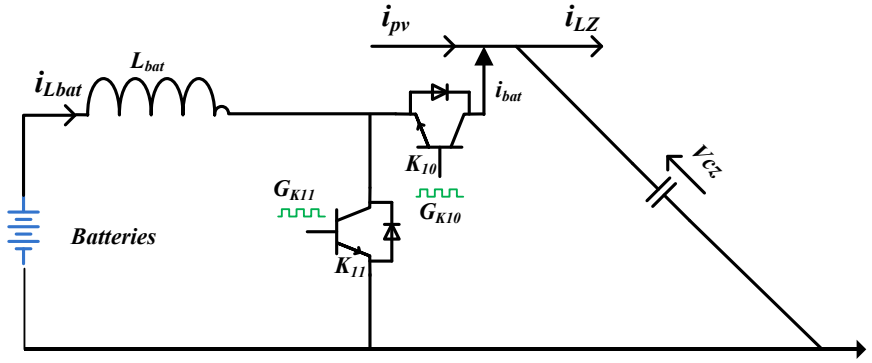

Figure 8: Buck-boost converter.

$$\begin{bmatrix} v_{Lbat}(t) \\ i_{cz}(t) \end{bmatrix} = \begin{bmatrix} -F_{K10} & 0 \\ 0 & F_{K10} \end{bmatrix} \begin{bmatrix} v_{cz}(t) \\ i_{Lbat}(t) \end{bmatrix} + \begin{bmatrix} v_{bat}(t) \\ -i_{lz}(t) \end{bmatrix} \tag{10}$$

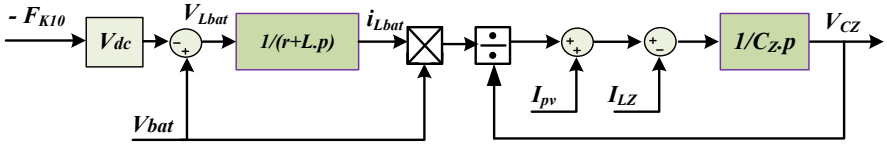

(a)

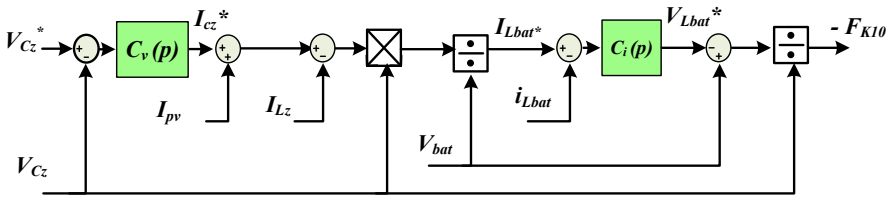

(b)

Figure 9: V_{cz} regulation schemes: a) Buck-boost model to control V_{cz}. b) Buck-boost converter control model.

The control model represented by Fig.9(b) is established from the average model (Fig.9(a)) to control the V_{cz} voltage.

To keep enough the output AC voltage control margin where there is a variation of irradiation or load power, the voltage level V_{cz} need to be readjusted to a desired value ${V_{cz}}^*$. To address this issue, the ZSI output AC voltages are controlled by keeping the reference capacitor voltage ${V_{cz}}^*$ as a variable. For this purpose, the exchange of energy between the storage system and the capacitor C_z must be adapted to the new reference voltage ${V_{cz}}^*$ through the buck-boost converter. The desired value ${V_{cz}}^*$ can be expressed as follows:

$$V_{CZ}^* = 2\hat{V_{ac}}\frac{1-D}{MD} \tag{11}$$

3.2. Operating mode selection

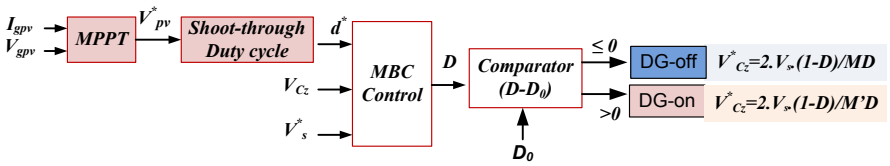

Figure 10: Mode selection logic.

To extract the maximum power from the PVG using a ZSI, the required shoot-through duty ratio D to achieve this MPPT is related on one hand to the system ability to follow the reference voltage ${V_{cz}}^*$ and on the other hand to the modulation index M fixed by the load power, which defines D_0. Therefore, and as shown by Fig.10, two operation modes can be considered for the system, the DG-off mode when ($D < D_0$) and the DG-on mode when ($D > D_0$).

3.2.1. DG-off Operating Mode

The controller objective in DG-off mode consist in controlling the ZSI so that it operates as a voltage source to ensure a constant voltage across the load in terms of amplitude and frequency. The voltage across the filter capacitor V_{cf} must be therefor regulated [3]. Using the model defined in (5), the V_{cf} voltage

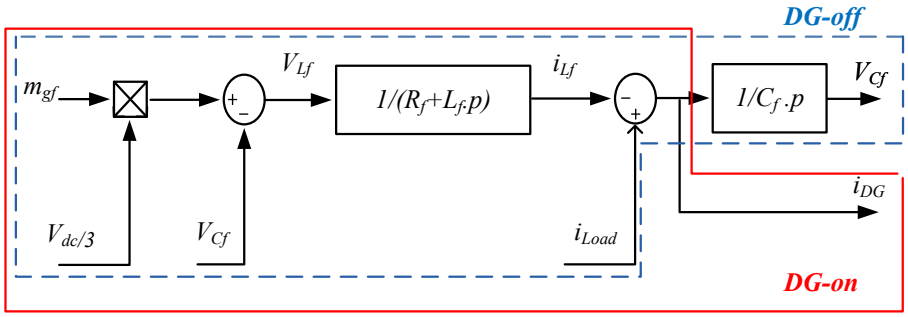

(a)

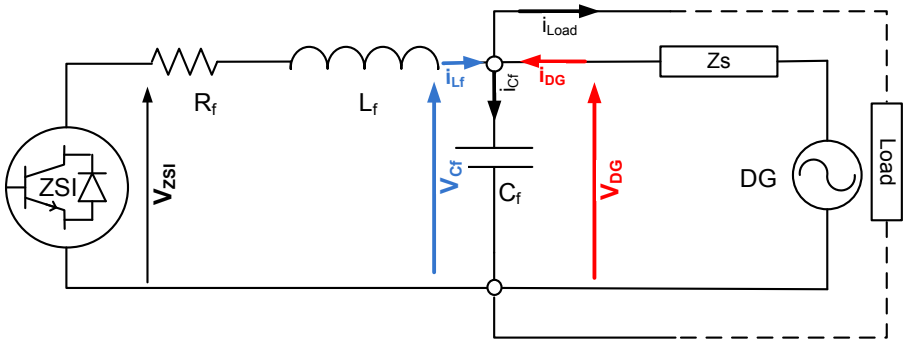

(b)

Figure 11: Simplified control model and synchronisation scheme: a) ZSI control model, b) Synchronisation scheme in DG-on mode.

can be described by the following equation system:

$$\begin{pmatrix} v_{Cf1} \\ v_{Cf2} \\ v_{Cf3} \end{pmatrix} = \begin{pmatrix} v_{an} \\ v_{bn} \\ v_{cn} \end{pmatrix} - \begin{pmatrix} L_f & 0 & 0 \\ 0 & L_f & 0 \\ 0 & 0 & L_f \end{pmatrix} \frac{d}{dt} \begin{pmatrix} i_{Lf1} \\ i_{Lf2} \\ i_{Lf3} \end{pmatrix} - \begin{pmatrix} R_f & 0 & 0 \\ 0 & R_f & 0 \\ 0 & 0 & R_f \end{pmatrix} \begin{pmatrix} i_{Lf1} \\ i_{Lf2} \\ i_{Lf3} \end{pmatrix} \tag{12}$$

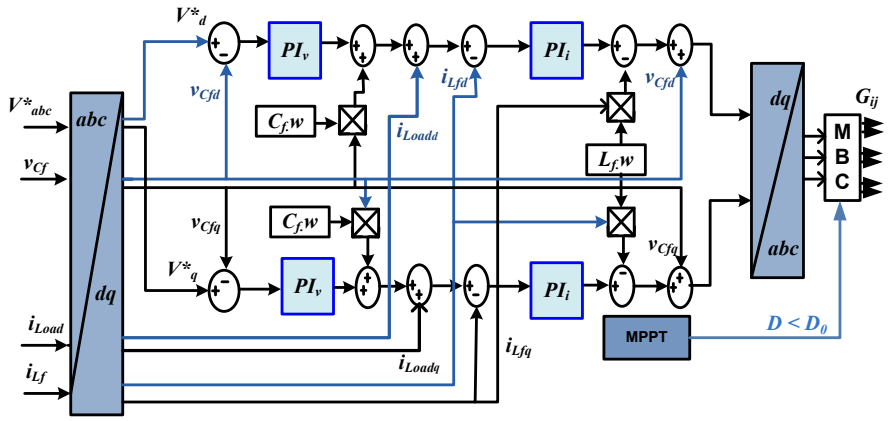

(a)

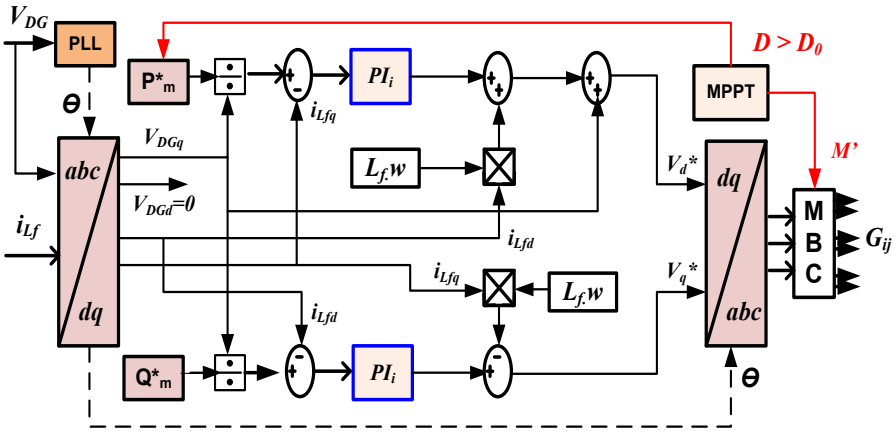

(b)

Figure 12: Proposed control strategy: a) Control strategy in DG-off mode, b) Control strategy in DG-on mode.

This model can be written in the $d-q$ reference frame as follows:

$$\begin{pmatrix} v_{Cfd} \\ v_{Cfq} \end{pmatrix} = \begin{pmatrix} v_d \\ v_q \end{pmatrix} - \begin{pmatrix} L_f & 0 \\ 0 & L_f \end{pmatrix} \frac{d}{dt} \begin{pmatrix} i_{Lfd} \\ i_{Lfq} \end{pmatrix} - \begin{pmatrix} R_f & 0 \\ 0 & R_f \end{pmatrix} \begin{pmatrix} i_{Lfd} \\ i_{Lfq} \end{pmatrix} \tag{13}$$

Figure.11(a) represents the ZSI model to regulate the voltages V_{cf}, where m_{gf} represents the matrix of the generating functions defined as follows:

$$m_{gf} = \begin{bmatrix} 2 & -1 & -1 \\ -1 & 2 & -1 \\ -1 & -1 & 2 \end{bmatrix} . \begin{bmatrix} F_{g11} \\ F_{g21} \\ F_{g31} \end{bmatrix} \tag{14}$$

where:

$$F_{g_{ij}} = \frac{1}{T} \int_{t-T}^{t} F_{ij}(t)\, dt \tag{15}$$

Figure 12(a) illustrates the control principle in DG-off mode. In the outer control loop, the reference voltage values are compared to the measured voltages V_{cf} to generate the reference values of currents in the inner control loop (${i_{Lfd}}^*$ and ${i_{Lfq}}^*$). The current controllers output is used to reconstruct the PWM switching strategy reference voltages, which determine the switching time of the active states, while the shoot-through duty ratio (D) is generated by the MPPT controller.

3.2.2. DG-on Operating Mode

In DG-off mode, the system can be in critical situations when the load current suddenly increases significantly, the AC output voltage regulation system generates a modulation index M, which may exceed the ratio set before. This increase in M, which results in an increase of the active states duration, will reduce the reference voltage level ${V_{cz}}^*$ and will consequently impact the AC output voltages. The DG-on operating mode is activated in this critical situation case when ($D > D_0$). Let us consider the new value of modulation index is: $M' = M - m$, the amplitude of AC output voltages can be formulted as:

$$\hat{V_{ac}} = M\frac{V_{dc}}{2} - m\frac{V_{dc}}{2} \tag{16}$$

When the ZSI and the DG are interconnected, the output voltages of the ZSI and the DG must have the same frequency, amplitude, and phase angle[32], [33, 34].

Figure 11(b) shows the equivalent circuit of the interconnected two sources. From this figure we can write:

$$\begin{cases} L_f \frac{d}{dt}(i_{Lf}) = v_{an} + v_{c_f} - R_f i_{Lf} \\ C_f \frac{d}{dt}(v_{Cf}) = i_{Lf} - i_{Load} \end{cases} \tag{17}$$

In the DG-on operating mode, the capacitor voltages V_{cf} are imposed by the DG. Equation (17) can thus be written in the following form:

$$\begin{cases} L_f \frac{d}{dt}(i_{Lf}) = v_{an} + v_{DG} - R_f i_{Lf} \\ i_{DG} = i_{Load} - i_{Lf} \end{cases} \tag{18}$$

As shown in Fig.12(b), the control strategy in DG-on mode needs to be analyzed in a rotational $d-q$ reference frame to calculate the phase angle (θ) of the DG output voltages. The active and reactive power's of the ZSI in the steady-state condition in a $d-q$ reference frame synchronized with the DG output voltages can be formulated as:

$$\begin{cases} P = V_{DGd} i_{Lfd} + V_{DGq} i_{Lfq} \\ Q = V_{DGq} i_{Lfd} - V_{DGd} i_q \end{cases} \tag{19}$$

Using Voltage Oriented Control (VOC), the reference values of currents (${i_{Lfd}}^*$ and ${i_{Lfq}}^*$) can be derived from the imposed reference powers P^* and Q^*. The proposed system uses a PI controller to regulate the measured currents i_{Lfd} and i_{Lfq} at their reference values.

$$\begin{cases} i^*_{Lfd} = \frac{P^*}{V_{DGq}} \\ i^*_{Lfq} = \frac{Q^*}{V_{DGq}} \end{cases} \tag{20}$$

The DG in this case is solicited to provide a minimum power of:

$$P_m = \frac{3mV_{dc}}{2\sqrt{2}} i_{Lf} \tag{21}$$

and the new value of M' can be rewritten as follows:

$$M' = M - \frac{2\sqrt{2}P_m}{3mV_{dc}\sqrt{(i^2_{Lfd} + i^2_{Lfq})}} \tag{22}$$

As mentioned earlier, the proposed controller for the ZSI in DG-on operating mode behaves as a current inverter to extract a minimum of power ($-P_m$) from the DG, nevertheless, and according to the load power, the DG can provide a supplementary power ($-P_{bat}$), which is used to charge the ESS according to the following equation:

$$P_{DG} = P_m + P_{bat} + P_{load} \tag{23}$$

Thus, according to the shoot-through duty ratio (D) generated by the MPPT controller, the control strategy in the DG-mode generates a new value of the modulation index (M') for the switching strategy (MBC) as well as the reference power ($P^* = -P_m - P_{bat}$) to be imposed for the DG.

Table 1: Simulation parameters.

PVG Parameters		DG Parameters	
PVG RP	3.2 kW	DG RP	10 kVA
Panel RP	135 W	T_v	0.03 sec
V_{oc}	21.8 V	T_d	0.05 sec
I_{cc}	8.17 A	ka	2.7
ns	9	D_T	0.1 pu
np	6	J_T	0.005 pu
ESS Parameters		ZSI Parameters	
V_{bat}	12 V	C_z	4.7 mF
C_{bat}	150 Ah	L_z	10 mH
r_{bat}	1 Ω	C_f	0.033mF
L_{bat}	0.05 H	L_f	4.8 mH

4. Simulation Results

In order to examine the performance of the proposed control strategy and verify the reported performance, we consider a typical hybrid system with bidi-

rectional ZSI. The system is modeled in MATLAB/Simulink taking into consideration irradiation and load changes. The ZSI, PVG, DG, and ESS simulation parameters are given in Table 1.

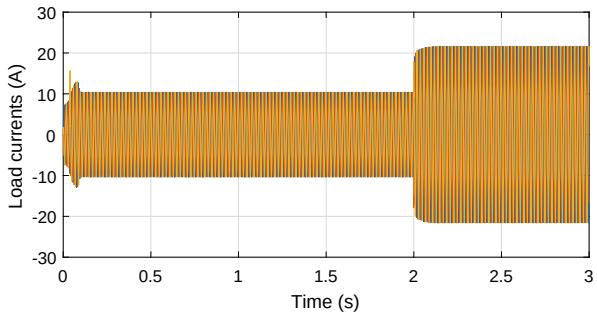

Figure 13: Load currents.

The voltage across the Z capacitors V_{cz}, is depicted in Fig.15(a) and Fig.15(b), respectively for DG-off mode and DG-on modes. These figures clearly show that the ESS controller succeeds to generate a reference voltage $V_{cz}{}^{*}$ of $622V$, which ensures an AC output voltage of $220V$.

The MBC control is used to generate the shoot-through duty ratio (D), required to achieve the MPPT. The maximum value of the modulation index (M) to control the AC output voltage is limited to 0.7. The system operation is investigated for both DG-off and on operating modes in order to verify that the critical issues in the DG-off mode can be solved in the DG-on mode. The irradiation profile and the PVG output power are depicted in Fig.14(a) and Fig.14(b), respectively. As shown in these figures, the ZSI is able to achieve the MPPT tracking in both DG-off and DG-on operation modes, for different irradiations and a constant temperature specified at $25^{0}C$. In both operating modes and for the same load profile as illustrated in Fig.13, the PVG output powers are the same with a better response time in the DG-on mode.

To evaluate the efficiency of the proposed control strategy, a sudden load change is applied at $t = 2s$ respectively for the two operating modes (Fig.13). As shown in Fig.15(a), the voltage stress across the Z capacitor in DG-off mode,

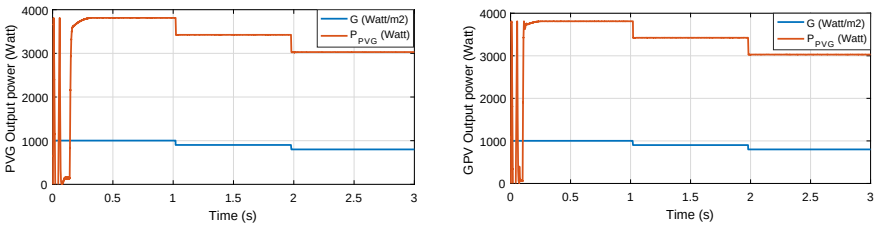

(a) (b)

Figure 14: PVG output power: a) DG-off mode, b) DG-on mode.

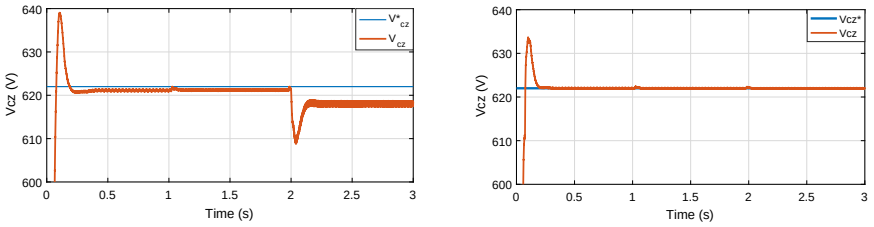

(a) (b)

Figure 15: Z-capacitor voltage: a) DG-off mode, b) DG-on mode.

need to be significantly decreased to ensure the shoot-through duty cycle required for the MPPT tracking. Therefore, as expected, the AC output voltages are impacted by this change.

Figure 16 shows that in the DG-on operating mode, the output voltages at AC side are imposed by the DG and the MPPT tracking in this mode can therefore be achieved without affecting the reference voltage across the Z capacitor V_{cz}.

Thus the DG can be solicited in critical situations in DG-off mode, which particularly highlights a better usage of the ZSI compared to other energy systems that do not use a DG. Fig.17(a) shows that the ESS is in discharge state in the DG-off mode with a positive current (i_{Lbat}) which is used to regulate the voltage across V_{cz}. At ($t = 2s$), the ESS delivers a important current to satisfy this request ($i_{Lbat} = 60A$); while for the DG-on mode, it is in charging state (Fig.17(b)) with a negative current depending on the DG generated power P_m

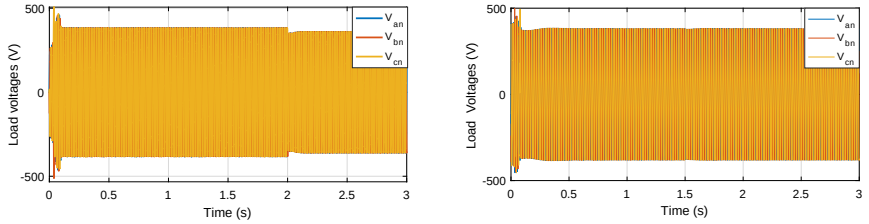

(a) (b)

Figure 16: Load voltages: a) DG-off mode, b) DG-on mode.

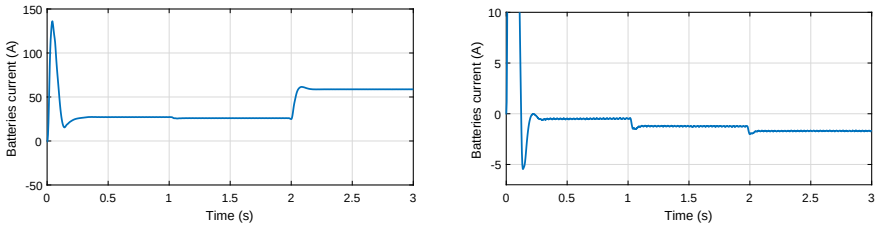

(a) (b)

Figure 17: ESS output current: a) DG-off mode, b) DG-on mode.

(Eq.21). In this case, the ZSI is controlled to transfer power from the AC side to the DC one.

Table 2: Test bench main components

Nb	Designation	Nb	Designation
1	Z-source network	2	Three-phases inverter
3	LC filter	4	Voltage and current sensors
5	PV panels	6	PC with PCI6280
7	Resistive load;	8	DC/DC converter and battery
9	DC Machine	10	3-phases synchonous generator
11	DC/DC converter (speed regulator)	12	DC/DC buck converter (AVR)
13	Speed sensor	14	Scope

5. Experimental results

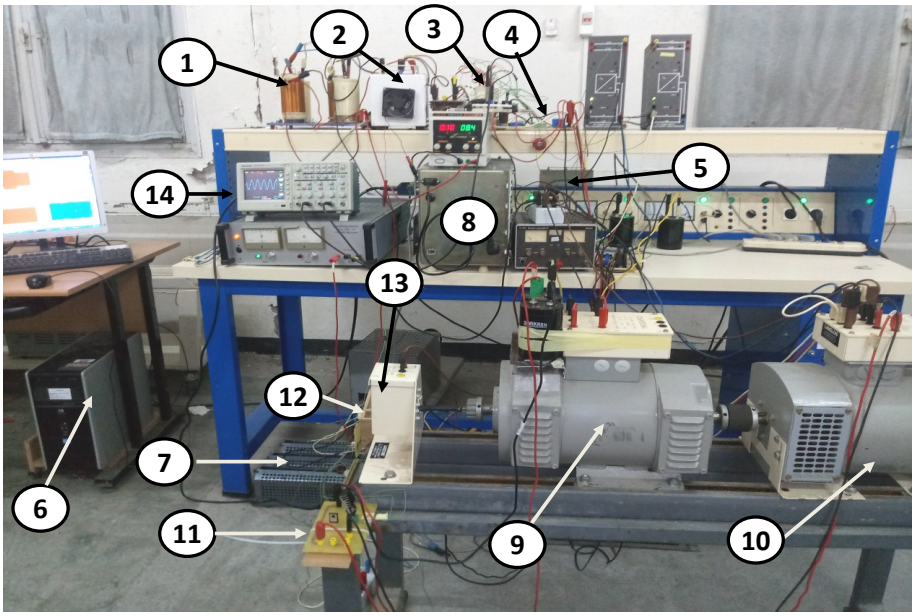

Figure 18: Experimental test bench.

For experimental validation, a reduced scale test rig has been developed (Fig.18). Its main components are listed in Table2. The power circuits correspond to the topology shown in Fig2.

5.1. Diesel Generator Emulator

A DG emulator has been designed and realized. This emulator is based on a DC machine and a three-phase synchronous generator (components 9 and 10 in Fig.18, respectively).

5.1.1. Speed Governor

The DC motor is supplied by a continuous DC source through a DC/DC buck converter (component 12), in order to maintain a constant driving speed under changing load. The rotation speed is regulated at a reference value of

1500rpm through the control of a the DC/DC buck converter (Fig.19). This requires a PI speed regulator with a good accuracy and a short response-time.

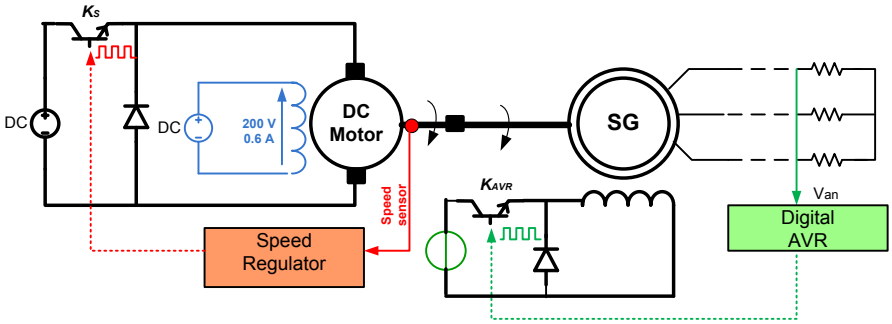

Figure 19: Simplified diagram of the DG emulator.

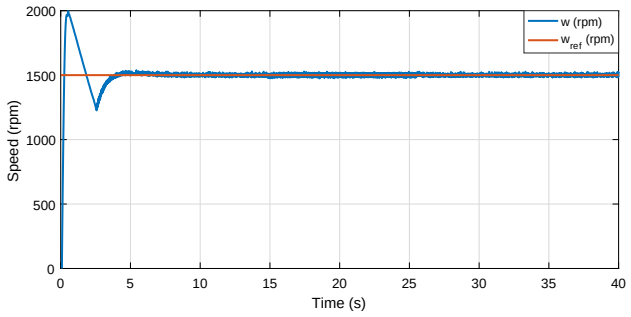

Figure 20: Speed governor performance.

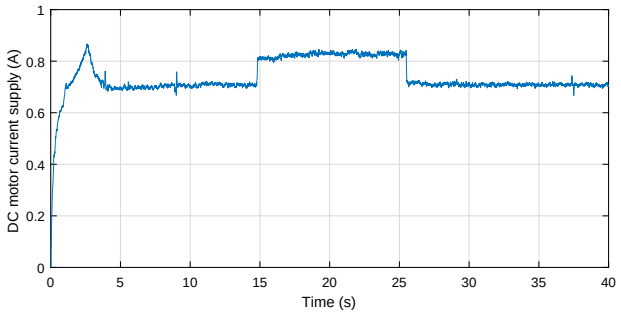

Figure 21: DC motor current supply.

Figure 20 shows the experimental dynamic response result of the speed gov-

ernor. When a large sudden load is applied at the AC bus (between 15s and 30s), the load torque T_e (applied by the synchronous machine) will exceed the torque produced by the DC motor (T_m). As shown by Fig.21, this torque deficit causes a decrease of the system speed before the governor increases the input current supplied to the DC motor through the control of the DC/DC buck converter. This transient regime continues until the DC motor being able to produce enough torque to accelerate to reach the rated speed, while the governor reduces the supplying current to its new steady-state value. In the same way and when a load disconnection occurs, an excess of the DC motor torque causes an increase of the system speed before the regulator acts to reduce the input current supplied to the DC motor to slow down the speed to its rated value. A direct consequence of this speed regulation is a stable frequency of the output voltages, according to the following equation:

$$\begin{cases} a = \frac{1}{J}\left(T_m - T_e\right) \\ \omega = \int a dt \end{cases} \tag{24}$$

Where, a is the system acceleration (rad/s), J is the combined inertia (Kgm^2) and ω is the system speed (rad/s^2)).

5.1.2. Automatic Voltage Regulator

The designed digital AVR controls the excitation voltage of the synchronous generator field winding through a DC/DC buck converter (Fig.19), in order to regulate the generator output voltage and to keep it constant by limiting as fast as possible the voltage peaks and overvoltages due to the load variations.

Figure 22 shows the emulator performance in terms of AC output voltages regulation. We can observe that the output voltages of the synchronous generator are well regulated to their reference value ($V_{RMS} = 80V$) through the control of switch K_S, thus validating the calculation process of the voltage regulator parameters and the control robustness against the load variations.

Figure 23 clearly shows that the rotor field winding is excited by a DC

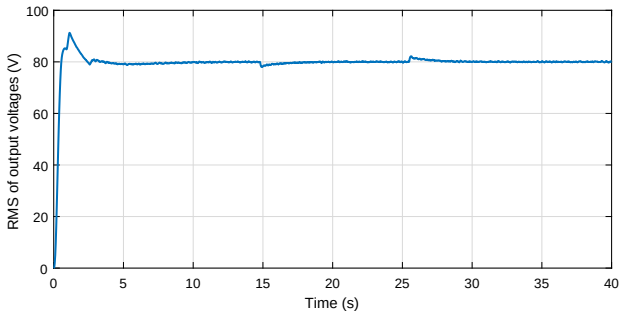

Figure 22: RMS of output voltages.

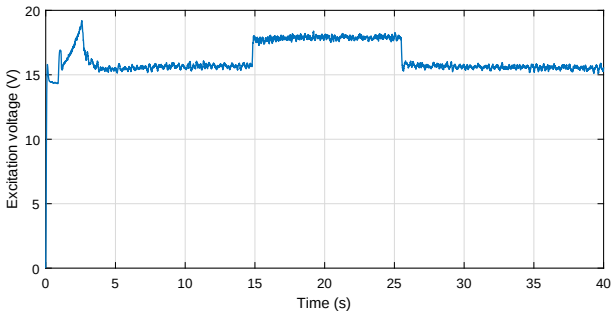

Figure 23: Excitation voltage.

voltage through the control of switch K_{AVR}. It is indeed through the generated magnetic flux that the AVR compensates the voltage droop of the fed load.

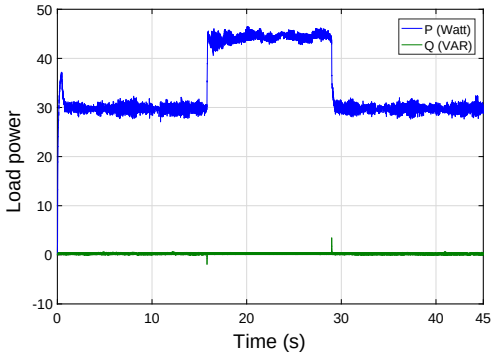

Figure 24: Load power profile.

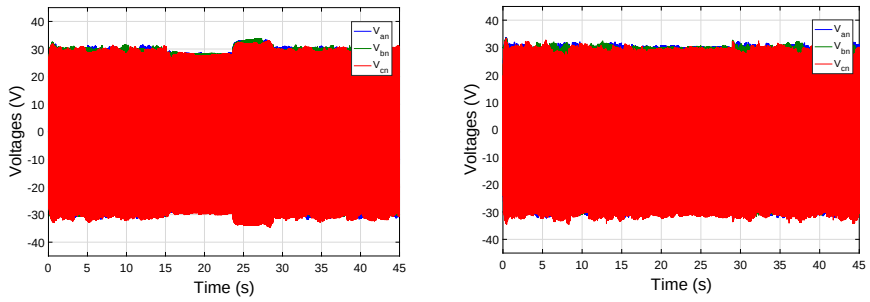

(a) (b)

Figure 25: Waveforms of AC voltages at PCC: a) DG-off mode, b) DG-on mode.

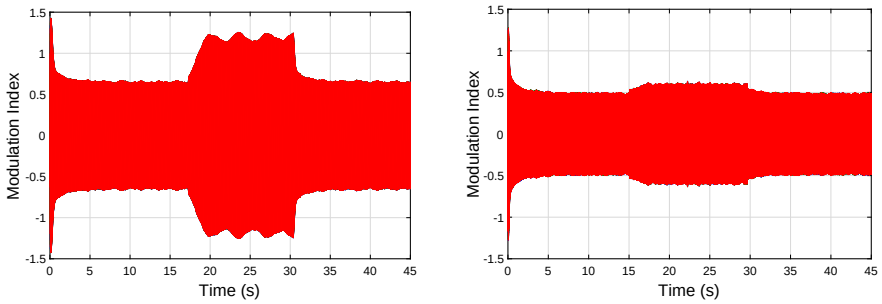

(a) (b)

Figure 26: Reference voltages for the switching strategy (MBC): a) DG-off mode, b) DG-on mode.

5.2. Experimental validation of DG-off and DG-on modes

Real-time experiments are carried out using a PCI6082E acquisition board, with several inputs/outputs. The used experimental validation parameters are listed in Table 3. The PWM pulses with shoot-through states from the MBC block are generated by the PCI6082E card and then sent out through six independent digital output channels to the inverter six switches gates. In the same way, the two PWM pulses from the V_{cz} voltage regulation block are sent

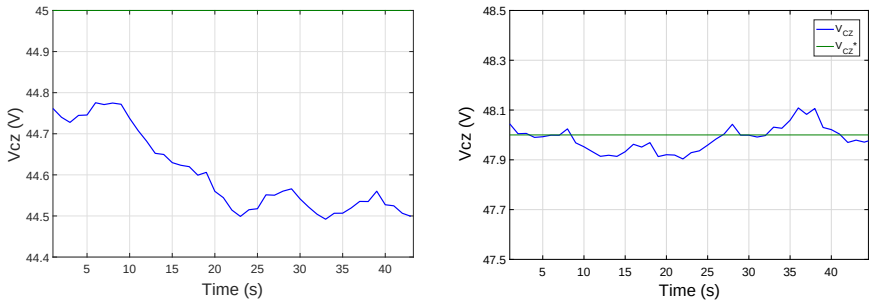

(a) (b)

Figure 27: Waveforms of experimental Z-capacitor voltage(V_{CZ}): a) DG-off mode, b) DG-on mode.

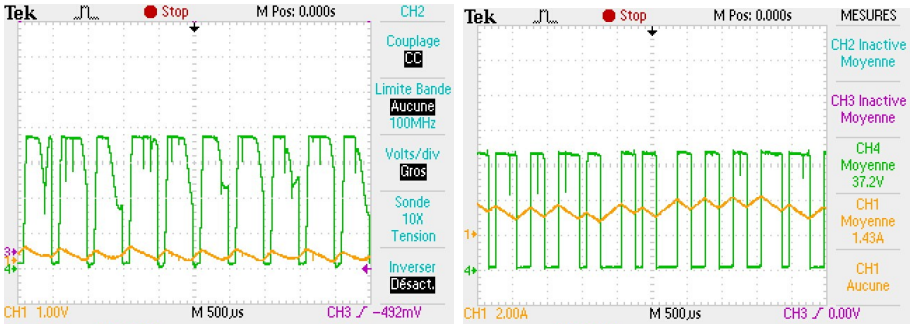

(a) (b)

Figure 28: Waveforms of DC bus voltage (V_{dc}) and i_{LZ} current: a) DG-off mode, b) DG-on mode.

315 out through two independent digital output channels to gate the buck-boost converter two switches gates.

The objective of the carried out tests is to demonstrate that in critical situations, when a peak load occurs, the DG-mode can improve the system operation and solve the DG-off mode deficits to achieve the MMPT tracking task. 320 Figure24 depicts the load power profiles of each operating mode. It can be calculated based on the output voltage and the load current waveforms.

Figures 25(a) and 25(b) show AC voltages at PCC for DG-off and DG-on

Table 3: Experimental validation parameters.

PVG Parameters		ZSI Parameters	
Panel RP	135 W	C_z	47 mF
V_{pv}^*	17.7 V	L_z	1 mH
V_{oc}	21.8 V	R_f	3.33 Ω
I_{pv}^*	7.67 A	L_f	32 mH
I_{cc}	8.17 A	C_f	$0.03mF$
ESS Parameters		DG Emulator Parameters	
V_{bat}	12 V	DC motor	$1.5kW$, $220V$, $9A$
C_{bat}	100 Ah	SG	$1.5kW$, $400V$, $2.9A$
n_{bat}	1	Speed sensor	$1500rpm$:$10V$

modes, respectively. The peak value of $30V$ correspond to a voltage reference ${V_{cz}}^* = 48V$ and a modulation index $M = 0.7$, taking into account the filter ohmic voltage drop. It can be observed that the ZSI output voltages are impacted in the first mode (DG-off) when another load is connected, as shown in Fig.26(a). This voltage drop results from the MBC control strategy overmodulation, since the reference voltages exceed the linear control area leading to a modulation ratio $M > 1$ ($M \simeq 1.2$). The shoot-through duty ratio D generated by the control scheme of Fig.12(a) is not sufficient to achieve MPPT and the voltage V_{CZ} need to be decreased as shown by Fig.27(a).

In the DG-on operating mode, it can be observed from Fig.25(b) that the voltages at PCC are well regulated, which clearly mean that the ZSI and DG output voltages are synchronized. The DG emulator is solicited in this mode when the second load is connected between 10 and $33s$ to keep the MBC strategy reference voltages in the linear control area. The new value of modulation index can be deduced from Fig.26(b) as: $M' = M - m = 1.2 - 0.45 = 0.75$. As discussed in Subsection.3.2.2, the shout-through duty ratio (D) generated by the control scheme of Fig.12(b) exceeds the limit value $D_0 = \frac{2\pi - 3\sqrt{3}.0.75}{2\pi} = 0.396$)

and the load power provided by the DG emulator can be expressed by Eq.22 .

In order to highlight the main merits of the proposed control strategy, the experimental waveforms of the input DC voltage source and source inductor current (i_{LZ}) are illustrated by Fig.28(a) and Fig.28(b) for DG-off and DG-on modes, respectively. It can be clearly observed that the active states are impacted in the first case.

6. Conclusion

This paper dealt with an efficient control strategy for a bidirectional Z-source inverter for a PV-diesel generator-energy storage hybrid system. The proposed control strategy is based on the voltage regulation across one of the Z-network capacitor through a buck-boost converter of the ESS side. It handles two operational control schemes: DG-off and DG-on modes controls. Indeed, in some critical situations, where the load power is important, the Z-network capacitor voltage regulation is no longer able to ensure the duration of the necessary state shoot-through for the MPPT achievement. In this context, the DG (DG-on mode) is therefore solicited to ensure the shoot-through duration and achieve MPPT so that it can be used more advantageously without any harmful effects on the Z-source inverter operation.

References

[1] M. F. Zia, E. Elbouchikhi, M. Benbouzid, Microgrids energy management systems: A critical review on methods, solutions, and prospects, Applied energy 222 (2018) 1033–1055.

[2] S. Sajadian, R. Ahmadi, Model predictive-based maximum power point tracking for grid-tied photovoltaic applications using a Z-source inverter, IEEE Transactions on Power Electronics 31 (11) (2016) 7611–7620.

[3] A. Belila, M. Benbouzid, E.-M. Berkouk, Y. Amirat, On energy management control of a pv-diesel-ess based microgrid in a stand-alone context, Energies 11 (8) (2018) 2164.

[4] A. Belila, Y. Amirat, M. Benbouzid, E. M. Berkouk, G. Yao, Virtual synchronous generators for voltage synchronization of a hybrid pv-diesel power system, International Journal of Electrical Power & Energy Systems 117 (2020) 105677.

[5] A. Belila, B. Tabbache, A control strategy of hybrid system diesel-photovoltaic-battery for stand-alone applications, in: Environment and Electrical Engineering (EEEIC), 2015 IEEE 15th International Conference on, IEEE, 2015, pp. 860–865.

[6] R. Abbassi, S. Saidi, M. Hammami, S. Chebbi, Analysis of renewable energy power systems: reliability and flexibility during unbalanced network fault, in: Handbook of research on advanced intelligent control engineering and automation, IGI Global, 2015, pp. 651–686.

[7] A. Belila, B. Tabbache, E.-M. Berkouk, M. Benbouzid, Integration of a storage system in a hybrid system" diesel-photovoltaic" for stand-alone applications, in: 2017 IEEE International Conference on Environment and Electrical Engineering and 2017 IEEE Industrial and Commercial Power Systems Europe (EEEIC/I&CPS Europe), IEEE, 2017, pp. 1–6.

[8] M. Cavalcanti, F. Bradaschia, M. de Melo Neto, G. Azevedo, T. Cardoso, Dynamic modeling and control system design of the buck-boost-based three-state three-phase z-source inverter, International Journal of Electrical Power & Energy Systems 104 (2019) 654–663.

[9] M. Alizadeh, S. S. Kojori, Small-signal stability analysis, and predictive control of z-source matrix converter feeding a pmsg-wecs, International Journal of Electrical Power & Energy Systems 95 (2018) 601–616.

[10] J. Khajesalehi, K. Sheshyekani, M. Hamzeh, E. Afjei, Maximum constant boost approach for controlling quasi-Z-source-based interlinking converters in hybrid AC-DC microgrids, IET Generation, Transmission & Distribution 10 (4) (2016) 938–948.

[11] N. S. González-Santini, H. Zeng, Y. Yu, F. Z. Peng, Z-source resonant converter with power factor correction for wireless power transfer applications, IEEE Transactions on Power Electronics 31 (11) (2016) 7691–7700.

[12] O. Husev, C. Roncero-Clemente, E. Romero-Cadaval, D. Vinnikov, T. Jalakas, Three-level three-phase quasi-z-source neutral-point-clamped inverter with novel modulation technique for photovoltaic application, Electric Power Systems Research 130 (2016) 10–21.

[13] S. Thangaprakash, Unified MPPT control strategy for Z-source inverter based photovoltaic power conversion systems, Journal of Power Electronics 12 (1) (2012) 172–180.

[14] W. Libo, Z. Zhengming, L. Jianzheng, A single-stage three-phase grid-connected photovoltaic system with modified MPPT method and reactive power compensation, IEEE Transactions on Energy Conversion 22 (4) (2007) 881–886.

[15] S. Sajadian, R. Ahmadi, Model predictive control of dual-mode operations Z-source inverter: Islanded and grid-connected, IEEE Transactions on Power Electronics 33 (5) (2018) 4488–4497.

[16] O. Ellabban, H. Abu-Rub, An overview for the z-source converter in motor drive applications, Renewable and Sustainable Energy Reviews 61 (2016) 537–555.

[17] Z. Liang, S. Hu, Y. Liu, W. Li, X. He, Application of bi-directional Z-source in ultracapacitor-battery hybrid energy storage system for EV, in: Applied Power Electronics Conference and Exposition (APEC), 2015 IEEE, IEEE, 2015, pp. 3124–3127.

[18] P. Liu, H. Liu, Permanent-magnet synchronous motor drive system for electric vehicles using bidirectional Z-source inverter, IET Electrical Systems in Transportation 2 (4) (2012) 178–185.

[19] S. Hu, Z. Liang, X. He, Ultracapacitor-battery hybrid energy storage system based on the asymmetric bidirectional Z-source topology for EV, IEEE Transactions on Power Electronics 31 (11) (2016) 7489–7498.

[20] E. Babae, H. Suryawanshi, H. Abu-Rub, Z-source converters: Topologies, modulation techniques, and applications. Part II, IEEE Transactions on Industrial Electronics 65 (10) (2018) 8274–8276.

[21] H. Mahmoudi, M. Aleenejad, R. Ahmadi, Modulated model predictive control for aZ-source based permanent magnet synchronous motor drive system, IEEE Transactions on Industrial Electronics 65 (10) (2018) 8307.

[22] E. Babaei, H. Abu-Rub, H. M. Suryawanshi, Z-source converters: Topologies, modulation techniques, and application. Part I, IEEE Transactions on Industrial Electronics 65 (6) (2018) 5092–5095.

[23] Y. Huang, M. Shen, F. Z. Peng, J. Wang, Z-source inverter for residential photovoltaic systems, IEEE Transactions on Power Electronics 21 (6) (2006) 1776–1782.

[24] Y. P. Siwakoti, F. Z. Peng, F. Blaabjerg, P. C. Loh, G. E. Town, S. Yang, Impedance-source networks for electric power conversion part ii: Review of control and modulation techniques, IEEE Transactions on Power Electronics 30 (4) (2014) 1887–1906.

[25] Y.-S. Kim, E.-S. Kim, S.-I. Moon, Frequency and voltage control strategy of standalone microgrids with high penetration of intermittent renewable generation systems, IEEE Transactions on Power systems 31 (1) (2016) 718–728.

[26] J. Zhang, Unified control of Z-source grid-connected photovoltaic system with reactive power compensation and harmonics restraint: design and application, IET Renewable Power Generation 12 (4) (2017) 422–429.

[27] O. Ellabban, H. Abu-Rub, Z-source inverter: Topology improvements review, IEEE Industrial Electronics Magazine 10 (1) (2016) 6–24.

[28] T. Li, Q. Cheng, A comparative study of Z-source inverter and enhanced topologies, CES Transactions on Electrical Machines and Systems 2 (3) (2018) 284–288.

[29] S. A. Singh, G. Carli, N. A. Azeez, S. S. Williamson, Modeling, design, control, and implementation of a modified Z-source integrated pv/grid/ev dc charger/inverter, IEEE Transactions on Industrial Electronics 65 (6) (2018) 5213–5220.

[30] A. Abdelhakim, P. Davari, F. Blaabjerg, P. Mattavelli, An improved modulation strategy for the three-phase Z-source inverters (ZSIs), in: Energy Conversion Congress and Exposition (ECCE), 2017 IEEE, IEEE, 2017, pp. 4237–4243.

[31] M. Mohammadi, J. S. Moghani, J. Milimonfared, A novel dual switching frequency modulation for Z-source and quasi-Z-source inverters, IEEE Transactions on Industrial Electronics 65 (6) (2018) 5167–5176.

[32] I. Grgić, M. Bašić, D. Vukadinović, Optimization of electricity production in a grid-tied solar power system with a three-phase quasi-Z-source inverter, Journal of Cleaner Production 221 (2019) 656–666.

[33] R. Abbassi, S. Marrouchi, S. Saidi, A. Abbassi, S. Chebbi, Optimal energy management strategy and novel control approach for dpgss under unbalanced grid faults, Journal of Circuits, Systems and Computers 28 (04) (2019) 1950057.

[34] R. Abbassi, S. Saadi, S. Marrouchi, S. Chebbi, Novel flexible algorithm for the operation of renewable source grid interface vscs under unbalanced voltage sags, in: 2015 IEEE 15th International Conference on Environment and Electrical Engineering (EEEIC), IEEE, 2015, pp. 1414–1419.